Presented at the 32nd European PV Solar Energy Conference and Exhibition, 20-24 June 2016, Munich, Germany

GENUINE BIFACIAL SIMULATION AND OPTIMIZATION OF AN MC-SILICON PERC SOLAR CELL

Nico Wöhrle, Aina Alapont Sabater, Johannes Greulich
Fraunhofer Institute for Solar Energy Systems ISE, Heidenhofstraße 2, 79110 Freiburg, Germany
Telephone: +49 761 4588 5964, fax: +49 761 4588 7621, e-mail: nico.woehrle@ise.fraunhofer.de

ABSTRACT: Bifacial silicon solar cells gain significantly in importance as they provide a plus in power generation for various illumination scenarios without significantly complicating the manufacturing process. These scenarios can be numerous and are hard to be fully covered in experimental setups. It is suitable to perform computer simulations to gain deeper understanding of the cell characteristics under wide parameter variations and to optimize the layout towards different applications. For this purpose, a numerical simulation model has been developed, which allows a genuine bifacial simulation, i.e., independently selectable illumination windows for both sides. The model is used to simulate a broad variation of different bifacial mc-Si PERC cell layouts under different illumination scenarios. It is shown that physical effects of the front and rear side grid do not couple in good approximation, so both grids can be adjusted independently. Further the simulations show that in case of the presented mc-Si PERC cell, it is possible to find a sweet spot of 110 front fingers and 130 rear fingers where the cell provides close-to-ideal power output under all applied bifacial illumination conditions as well as a broad range of minority carrier lifetimes and base resistances.
Keywords: bifacial solar cell, multi-crystalline, PERC, Sentaurus Device simulation, PV Lighthouse

1 INTRODUCTION

The topic of bifacial passivated emitter and rear cells (biPERC, [1–3]) is supposed to be the next step in PERC [4] evolution after monofacial PERC technology successfully entered industrial mass production. With a predicted market share of 30% for bifacial silicon modules in 2026 [5] it is time to push advance-development of bifacial PERC technology. Simulation studies are no niche in PV R&D anymore but contribute substantially to the development in solar cell physics and technology. As bifacial simulation is a new field, there is a need for respective models, especially as bifacial characterization techniques are only just being evolved.

We want to provide the models for genuine bifacial simulation and show an extensive study on this topic in order to indicate the solar cell's behavior in power generation under several illumination scenarios for a large number of design variations and to give guidelines for the design of bifacial multi-crystalline (mc) PERC. The Sentaurus Device [6] models presented here are working truly bifacial, i.e., with two separately configurable illumination sources. Such simulations may generate a resilient basis for the upcoming discussion about bifacial measurement standards and rear side illumination spectra as the rear side AM1.5G spectrum may be easily replaced with optional albedo reflection in the simulation.

2 APPROACH

We equip the standard Sentaurus Device 2D models for solar cell simulation [7] with a second illumination source at the rear side which is adjustable in spectrum and intensity independent from the front illumination. The approach suits 3D models likewise. Using this model, we perform simulations with up-to-date input parameters for a bifacial p-type mc-PERC solar cell as described in section 4. The cell features a lately (at Fraunhofer ISE) developed phosphorus-doped emitter with sheet resistance R_{sh} = 85 Ω/sq and a screen-printed aluminum-boron back surface field (AlB-BSF) [8] beneath line-shaped laser contact openings (LCO [9]). The large parameter space for this study comprises independent intervals for the front- and rear-side finger numbers, three different rear-side finger widths, two base resistances, four bulk minority carrier lifetimes, and five different illumination conditions (for cell and module optics) representing a south-facing orientation with different rear intensities and an east/west-facing orientation.

3 MODEL

3.1 Technical setup

As for most Sentaurus Device simulations, the modeling is a two-step process: Starting with a pure optical ray tracing simulation, a spectrally and depth-resolved carrier generation profile is created. This carrier profile is injected into an electrical model where the voltage is ramped through the contacts generating the illuminated current-voltage curve.

To extend this routine towards bifacial illumination a second, independent optical simulation is conducted with a rear side illumination source permitting all different kinds of rear side spectra (albedo ground reflection, diffuse ambience radiation, AM spectra with optional intensities). Several generation profiles are joint in one electrical model, each one arranged according to its designated illumination source. The detailedness of illumination regions can be chosen as far as it is necessary or suitable. In this work, we differentiate not only between front and rear side generation but also between front side generation above rear contacts, above passivated rear metallization and above rear passivation (open rear side). Fig. 2 demonstrates a step-wise implementation of generation profiles into the electrical symmetry element. We call this modelling approach "genuine" bifacial simulation as the achievable degree of precision is unique so far and helpful for optimizing the layout of bifacial solar cells.

3.2 Illumination scenarios

Using the bifacial simulation model developed here, different illumination scenarios shall be used for the optimization of a bifacial mc-PERC solar cell presented in section 4. The following two scenarios represent a simple approach of a bifacial solar cell/module in two spatial orientations, visualized by Fig. 2:

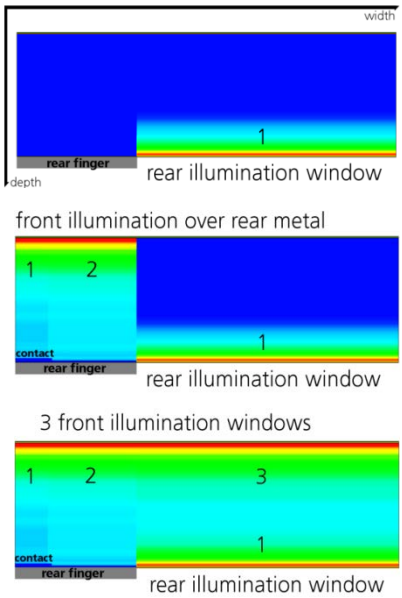

Fig. 1. a) Electrical symmetry element with implemented generation profile arising from rear illumination.
b) additional implementation of front generation over the rear contact and the metal finger (with passivation).
c) additional implementation of front generation over the rear side passivation.

1. "Standard" elevation towards the south (1000 W/m² front illumination) with different illumination intensities from the rear side: 100, 250, 500 W/m² (each with AM1.5G spectrum)
2. Vertical elevation towards east/west represented by averaging a) 750 W/m² front and 250 W/m² rear and b) 250 W/m² front and 750 W/m² rear illumination (each with AM1.5G spectrum)

For module optics a both-sided encapsulation of 0.45 mm EVA and 3 mm glass are added as specified in Table I.

3.3 Discussion

Besides the described advantage of a detailed differentiation of optical generation and adaption to numerous illumination conditions, there is currently one discussable weakness of the model: As can be seen in Fig. 1, the borders of the generation profiles in the different cell regions are vertical to the cell surface, which neglects e.g. generation beneath fingers due to angular incidence of light. We currently seek a technical option to solve this. Note that optical refraction due to texturing and multiple light bounces beneath the open rear side region are fully included in the optical simulation and therefore appropriately represented in the optical generation profile. Note that the electrical model in Fig. 1 shows carrier generation, not light paths.

4 OPTIMIZATION OF AN MC-PERC SOLAR CELL

We want to use the presented model to show an optimization of a bifacial multi-crystalline PERC with LCO contacts and a local AlB-BSF on a 156 mm large wafer. The cell's features are listed in Table I. The minority carrier lifetime is set to $\tau_{SRH} = 100$ µs if not stated otherwise.

As there are currently no norms for efficiency calculation with bifacial illumination, all results are given in output power density units P_{out} (mW/cm²).

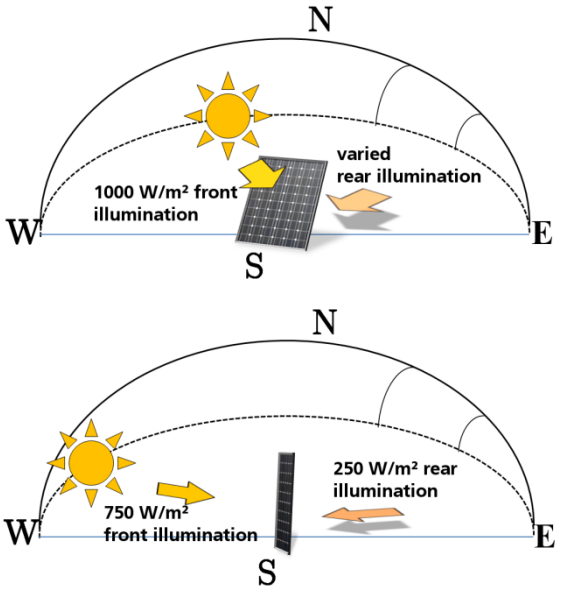

Fig. 2. a) Illumination scenario *"south"*: front illumination 1000 W/m², varied rear illumination (100, 250, 500 W/m²).
b) Illumination scenario *"east/west"*: 750 W/m² front illumination, 250 W/m² rear illumination and vice versa.

4.1 Front side grid

The number of front fingers is varied between $n_{f\_FS} = 80$ and 140 while the number of rear side fingers is kept fixed at $n_{f\_RS} = 100$ in this step. Illumination scenario 1 (see section 3.2) is applied. Two different finger widths (75, 100 µm) are tested for the rear side; the base resistivity is 1.0 and 2.5 Ωcm.

A. Cell optics (no encapsulation)

Fig. 3 shows the resulting differences in output power in dependence of the finger variations for different rear

Table I: Simulated mc-PERC parameters;

characteristic angle ω, layer thickness d, depth z, specific finger resistance ρ_f, specific contact resistance ρ_c, optical constants n & k, finger width w_f, finger height h_f, emitter sheet resistance R_{sh}

front		rear	
iso-texture	ω = 60°, z = 3.6 µm	iso-texture	ω = 60°, z = 3.6 µm
j_{0e}	75 fA/cm²	j_{0bsf}	350 fA/cm²
$j_{0e,met}$	1200 fA/cm²	d_{bsf}	3 µm
R_{sh}	85 Ω/sq	d_{Al2O3}/d_{SiNx}	10/70 nm
d_{SiNx}	75 nm	S_{pass}	10 cm/s
front grid		rear grid	
h_{f_front}	20 µm	h_{f_rear}	25 µm
w_{f_front}	54 µm	w_{f_rear}	varied
ρ_{f_front}	5.94 µΩcm	ρ_{f_rear}	20 µΩcm
ρ_{c_front}	6 mΩcm²	ρ_{c_rear}	3 mΩcm²
encapsulation			
d_{EVA}	0.45 mm	n_{EVA}	see [10]
		k_{EVA}	see [10]
d_{glass} (borosilicate glass)	3 mm	n_{glass}	1.5
		k_{glass}	See [11]

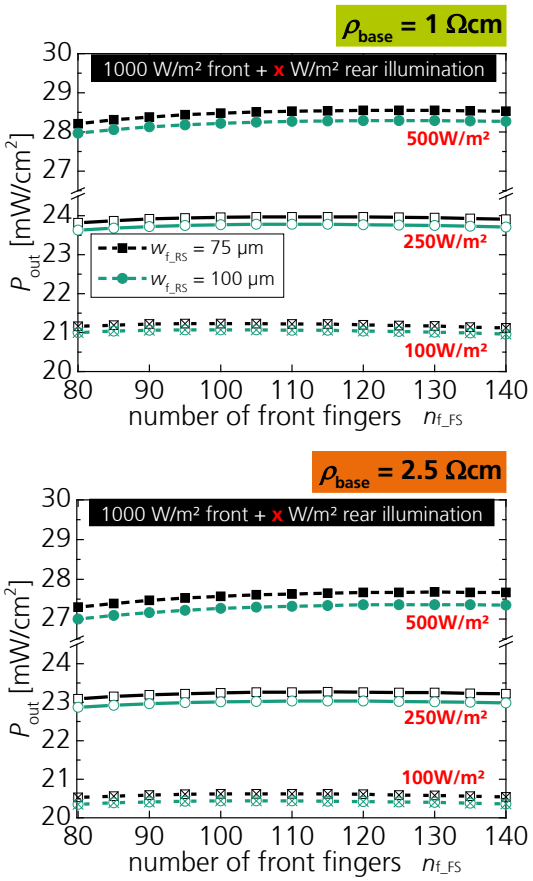

Fig. 3. Output power P_{out} as a function of the number of front fingers, calculated with cell optics for two rear finger widths w_{f_RS} = 75 µm and 100 µm. The cell is illuminated by constant front (1000 W/m²) and three different rear intensities (100, 250, 500 W/m²).

illumination intensities. The layout-induced deviations in P_{out} over n_{f_FS} are below 0.3 mW/cm² for all plotted lines. In a more reasonable interval between 90 and 120 front fingers, they do not exceed 0.15 mW/m². It can be stated that in said interval the chosen number of front fingers will not have a substantial influence on P_{out} and is to a large degree independent from base resistivity. Moreover, it is quasi-independent from rear side illumination intensity. The front and rear grid optimization is therefore uncoupled.

B. Module optics (with encapsulation)

The same counts for module optics (with EVA and glass encapsulation). The encapsulation leads to a quite constant offset in optical generation compared with cell optics depending on the additional rear illumination. The variations ΔP_{out} in the output power range on module level between -0.15 and -0.4 mW/cm² for rear illumination intensities of 100 and 500 W/m², respectively, which is not plotted for clarity reasons.

4.2 Optimization of rear side capping

The rear side optimization begins with the thickness of the passivation capping as it is independent from the grid layout. The thickness of the SiN_x passivation layer is varied between d_{SiNx} = 30 nm and 120 nm to find the optimal value for different illumination conditions. d_{Al2O3} = 10 nm is kept constant. Due to the comfortable interface this optical simulation is performed with the

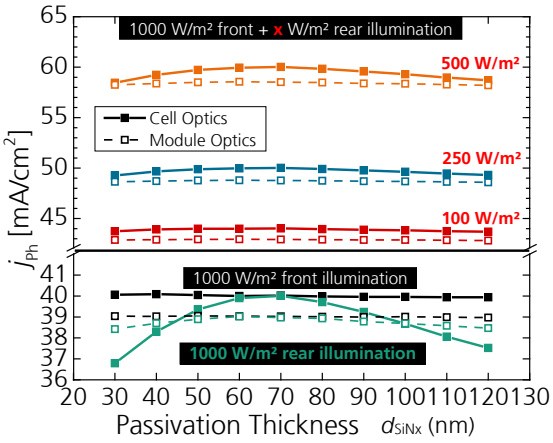

Fig. 4. Photocurrent density as a function of the thickness of the SiN_x capping layer within an Al_2O_3/SiN_x based rear side passivation stack with fixed Al_2O_3 thickness. Both sides are iso-textured. The lower third shows pure front illumination (black symbols) and pure rear illumination (green symbols). The upper two thirds show front plus rear illumination for varied rear intensities. Cell optics are plotted with solid lines, module optics with dashed lines.

PV Lighthouse "Module ray tracer" [12]. Other cell parameters remain unchanged to the previous simulations. As the ray tracer only supports front illumination, the cell structure is flipped to simulate rear illumination. Simultaneous illumination is calculated by addition of the integrated charge carrier generation rate j_{Ph} of different scenarios.

A. Cell optics

As visualized in the lower part of Fig. 4, the j_{Ph} generated by pure front illumination (black symbols) is almost independent from the SiN_x thickness of the rear side. In contrast j_{Ph} from rear illumination (green symbols) heavily depends on the SiN_x thickness with its peak at 70 nm.

The joint calculation with 1000 W/m² front and varied rear illumination (upper part of Fig. 4) therefore also shows its maxima at d_{SiNx} =70 nm, while the peak gets more pronounced the higher the portion of the rear illumination is.

B. Module optics

Adding 0.45 mm EVA and 3 mm glass does not shift the peak at d_{SiNx} = 70 nm but flattens it strongly. The maximum deviation in j_{Ph} for pure rear illumination (green symbols) in the SiN_x thickness interval between 30 nm and 120 nm decreases from 3 mA/cm² (on cell level) to 0.5 mA/cm² (on module level). For the joint calculation of front and rear illumination, a deviation of Δj_{Ph} < 0.3 mA/cm² over the regarded d_{SiNx} interval remains.

4.3 Optimization of rear side grid

As a next step, the rear side grid layout is optimized under consideration of several illumination conditions taking into account cell and module optics.

A. Cell optics

Again illumination scenario 1 (section 3.2) is applied to calculate the output power of the PERC cells as a function of the number of rear fingers, the width of the rear fingers being varied threefold with w_{f_rear} =75, 100 and 200 µm and base resistance of the substrate being

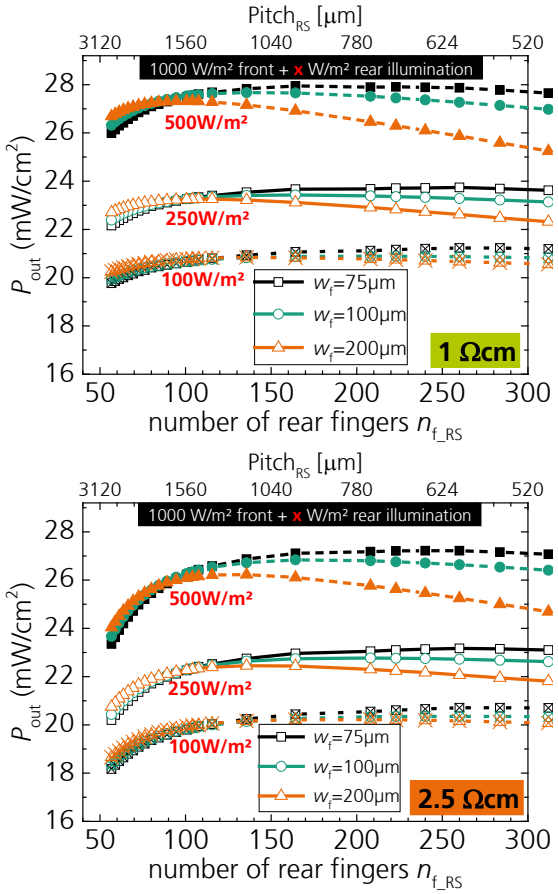

Fig. 5. Output power P_{out} on cell level as a function of the number of rear fingers for different finger widths w_{f_rear} = 75, 100, 200 µm and different base resistivities ρ_{base} = 1 and 2.5 Ωcm. The cell is illuminated by constant front (1000 W/m²) and three rear intensities (100, 250, 500 W/m²).

varied twofold with ρ_{base} = 1 and 2.5 Ωcm The results are plotted in Fig. 5. For w_{f_rear} = 75 µm (black symbols) and 100 µm (green symbols), the optima are located between 200 and 120 fingers for ρ_{base} = 1 Ωcm and between 260 and 160 fingers for ρ_{base} = 2.5 Ωcm and decrease with rear illumination intensity. While the intervals may seem large, the curves are very flat in these intervals showing a maximum deviation of only 0.3 mW/cm². For w_{f_rear} = 200 µm (orange symbols), which is the more common Al-finger thickness at the moment, the peaks shift towards lower finger numbers in the range of n_f = 150-100 due to higher shading of the rear side and thus lower j_{SC} towards increasing n_f.

The main differences between ρ_{base} = 1 and 2.5 Ωcm are a) a steeper drop in *FF* towards lower finger number due to increased spreading resistance for 2.5 Ωcm, which is visible in the larger bend of P_{out} between 50 and 100 fingers and b) a general offset in V_{OC} by about 10 mV leading to ~0.8 mW/cm² power loss for wafers with higher base resistivity caused by lower built-in voltage.

B. Module optics

As already seen in the front optimization (section 4.1), including module optics provides a general offset in j_{Ph} and thus P_{out} of -0.2 to -0.4 mW/cm² with increasing rear intensity, but does not alter the observed shapes.

4.4 Lifetime variation and east/west illumination

Illumination scenario 2 (see section 3.2) and a variation of bulk minority carrier lifetime between τ_{SRH} = 30 and 500 µs round up the simulation study which is shown in Fig. 6. This one is only performed for cell optics as module optics are not expected to yield different results than in the previous sections.

The east/west illumination scenario shows the largest dependency on the number of rear fingers and rear finger thickness, as the proportion of rear illumination is the highest in this case. Nevertheless, if the minority lifetime is higher than 250 µs, it almost yields the power output of the 1000 W/m² front illumination when choosing the optimal finger number of $n_{f\_RS} \approx$ 100-120. Lower bulk lifetimes increase the gap between front illumination and bifacial illumination (each with 1000 W/m² sum).

Another result is that the ideal rear layout for monofacial applications is a very high finger number exceeding the examined range (n_{f_RS} > 300). This means a rear layout optimized for monofacial application in this way would not be suited for bifacial application. However, a rear layout with n_{f_RS} = 110 rear fingers which is optimized for all examined bifacial scenarios, is very well suited for monofacial application as well as the deviations in P_{out} are below 0.3 mW/cm² between 100 and 300 fingers.

5 DISCUSSION

An important side note and motivation for the development of the simulation model is the non-existence of bifacial measurement norms. The relevant question of suitable measurement conditions is nevertheless beyond the scope of this publication. However, the simulations provide additional scientific insight into the underlying physical phenomena which may promote this ongoing discussion. The optimization of the mc-PERC layout is our first result which is directly applicable to bifacial cell technology.

The four steps of the simulation experiment reveal a remarkable robustness of the cell concepts towards varying material and illumination parameters if the layout is chosen correctly. The very small impact of the number of front fingers, as shown in Fig. 4, originates from the fact that the increase in *FF* (less lateral emitter resistance) compensates to a large degree for the decrease in V_{OC} (higher contact recombination) and j_{SC} (more shading) level. As these are all emitter or front surface effects neither base resistance nor rear illumination have qualitative influence on this behavior.

The rear capping layer optimization of this study focusses solely on optics. As the front illumination has negligible influence, the optimum always stays at the rear side optimum of 70 nm (together with 10 nm Al_2O_3), which is expected. Notice that this value may change if the spectral distribution of the rear illumination changes, as it is an optimized layer thickness for AM1.5G. Nevertheless, the peak is strongly flattened by module optics (Fig. 4), that this stack could be a decent choice for different albedo reflections as well. The flat peak indicates that the capping layer thickness may be adjusted for best electrical properties.

The optimization of the rear grid shows that in general the P_{out} deviation over finger number is small in a reasonable interval between 100 and 200 fingers especially for realistic rear illumination intensities

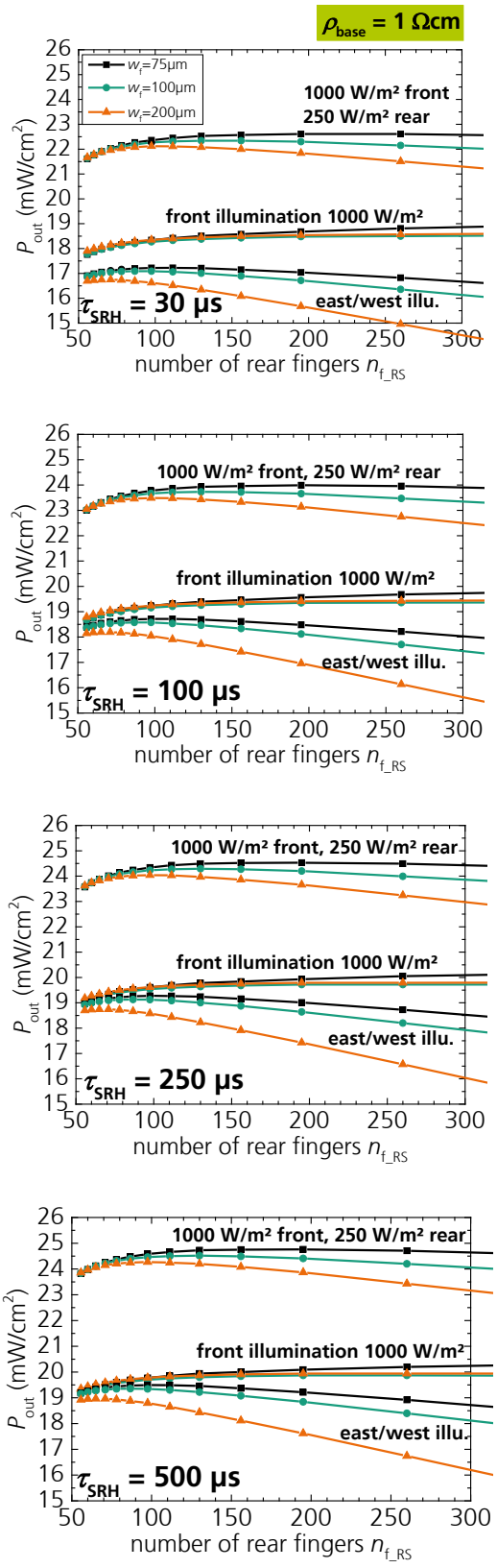

Fig. 6. Output power P_{out} on cell level as a function of the number of rear fingers. Lifetime variation τ_{SRH} = 30-500 µs for illumination scenario 1 (1000 W/m² + 250 W/m²), scenario 2 (east/west illumination) and monofacial illumination (1000 W/m²). Calculated with cell optics. Colors indicate different rear finger widths.

between 100 and 250 W/m². Thus, the exact finger number should not be the biggest concern and can be chosen according to individual preferences. Higher finger number has advantages towards process reliability, e.g. in case of finger interruptions. Less fingers may save costs. Also not much care has to be taken for base resistance concerning the layout as it mainly influences the quality of the power curve for low finger number – aside from the peak region – due to increasing spreading resistance. Two relevant aspects are observed: Firstly, for applications where the rear to front illumination ratio is large (e.g. east/west scenario, visible in Fig. 6), the rear finger number should be corrected towards smaller values. Secondly, thin Al fingers on the rear are desirable as they allow for more rear fingers, which improves the power output for higher base resistance material due to the reduced spreading resistance in the base. This can be beneficial for base resistance gradients over a group of wafers.

Finally, the variation of the SRH lifetime of the minority carriers between 30 and 500 µs and the introduction of the east-west scenario confirms the robustness of the chosen layout. There is no qualitative deviation to the optimum of 100-150 rear fingers which has been found in section 4.3. Moreover, the simulations show that the output power decreases significantly with decreasing bulk lifetime for all bifacial application, while it remains quite stable for monofacial application in the investigated lifetime range. The reason is that the investigated device exhibits a pn-junction at the front side, which leads to a reducted collection efficiency of carriers which are generated at the rear side compared to generation at the front due to higher recombination losses in the base.

6 CONCLUSION

The successful implementation of several independent illumination sources in one simulation setup was shown to provide a genuine bifacial simulation model. The introduced simulation model for bifacial mc-PERC cells has been used for a comprehensive parameter variation.

As a first result, we showed that, in an interval of 80-140 front fingers, front and rear finger numbers can be varied independently without coupling effects under 1000 W/m² (AM1.5G) front illumination in addition with 100 to 500 W/m² (AM1.5G) rear illumination. This counts for base resistances from ρ_{base} = 1 to 2.5 Ωcm as well as the applied rear side finger widths from 75 to 200 µm. This conclusion may ease the development of metal grid layouts to a great extent.

Further, we provided plots for variations of parameter sets that cover a wide range of possible cell configurations. One of the key findings was, that there is a sweet spot of rear side finger numbers at 110 fingers (ρ_{base} = 1 Ωcm) and 120 fingers (ρ_{base} = 2.5 Ωcm), which suits all investigated bulk lifetimes, finger widths and illumination scenarios. Thus, it is possible to build a bifacial mc-PERC solar cell that universally suits most irradiance scenarios with a max. loss of 0.35 mW/cm² to the single individual optimum configurations. We also showed that lifetime variations have negligible influence on the optimal cell layout. Base resistance variations have an impact but only a small one. The rear finger number should be optimized especially when dealing with high

rear to front illumination ratios. Further, thin fingers of around 100 µm should be a development goal, as such a layout allows for larger finger counts on the rear side. The outcome for the optimal design of the examined mc-PERC cell with 85 Ω/sq phosphorus-doped emitter and LCO rear contacts shows to be a 1 Ωcm base with high lifetime, 110 silver front fingers with 54 µm width and 5 busbars with a width of 500 µm. The rear side layout should have 100 Al-fingers of 200 µm width (today's standard) or 120 fingers of 100 µm or even 75 µm width as a development goal. These design rules for the rear side are lifetime-invariant and apply for cell optics as well as module optics with EVA and glass encapsulation.

ACKNOWLEDGEMENTS

The authors acknowledge the funding of the German Federal Ministry for Economic Affairs and Energy (BMWi) in the frame of the project "BiZePS" (contract number 0325909) and thank the associated project partners h.a.l.m. Elektronik GmbH and SolarWorld Innovations GmbH for the excellent cooperation.

REFERENCES

[1] Y. Chevalier and I. Chambouleyron, "Getting more power out of silicon," in *Proceedings of the 1st European Commission Conference on Photovoltaic Solar Energy*, pp. 977–986.

[2] K. Krauß, F. Fertig, J. Greulich, S. Rein, and R. Preu, "biPERC silicon solar cells enabling bifacial applications for industrial solar cells with passivated rear sides," *Phys. Status Solidi A*, vol. 213, no. 1, pp. 68–71, 2016.

[3] T. Dullweber *et al*, "PERC+: industrial PERC solar cells with rear Al grid enabling bifaciality and reduced Al paste consumption," *Prog. Photovolt: Res. Appl*, pp. n/a, 2015.

[4] A. W. Blakers, A. Wang, A. M. Milne, J. Zhao, and M. A. Green, "22.8% efficient silicon solar cell," *Applied Physics Letters*, vol. 55, no. 13, p. 1363, 1989.

[5] SEMI, "International Technology Roadmap for Photovoltaic (ITRPV)," Seventh Edition, Mar. 2016.

[6] Synopsys, "Sentaurus Device User Guide," vol. H-2013.03.

[7] P. P. Altermatt, "Models for numerical device simulations of crystalline silicon solar cells—a review," *J Comput Electron*, vol. 10, no. 3, pp. 314–330, 2011.

[8] M. Rauer, C. Schmiga, M. Glatthaar, and S. W. Glunz, "Alloying From Screen-Printed Aluminum Pastes Containing Boron Additives," *IEEE J. Photovoltaics*, vol. 3, no. 1, pp. 206–211, 2013.

[9] R. Preu *et al*, "Laser ablation - a new low-cost approach for passivated rear contact formation in crystalline silicon solar cell technology," in *16th EU PVSEC*, 2000, pp. 1181–1184.

[10] K. R. McIntosh *et al*, "An optical comparison of silicone and EVA encapsulants for conventional silicon PV modules: A ray-tracing study," in *2009 34th IEEE Photovoltaic Specialists Conference (PVSC)*, pp. 544–549.

[11] *PV Lighthouse - Refractive Index Library*.

[12] PV Lighthouse, *Module ray tracer*, 2016.